frontiers in Pharmacology

ORIGINAL RESEARCH
published: 22 November 2017
doi: 10.3389/fphar.2017.00852

Electrophysiological and Pharmacological Analyses of $Na_V1.9$ Voltage-Gated Sodium Channel by Establishing a Heterologous Expression System

Xi Zhou[1†], Zhen Xiao[1†], Yan Xu[1], Yunxiao Zhang[1], Dongfang Tang[1], Xinzhou Wu[1], Cheng Tang[1,2], Minzhi Chen[1,2], Xiaoliu Shi[3], Ping Chen[1,2], Songping Liang[1,2*] and Zhonghua Liu[1,2*]*

[1] National & Local Joint Engineering Laboratory of Animal Peptide Drug Development, College of Life Sciences, Hunan Normal University, Changsha, China, [2] Key Laboratory of Protein Chemistry and Developmental Biology of the Ministry of Education, College of Life Sciences, Hunan Normal University, Changsha, China, [3] Laboratory of Clinical Diagnosis and Research, Department of Medical Genetics, Second Xiangya Hospital of Central South University, Changsha, China

OPEN ACCESS

Edited by:
Brian McCool,
Wake Forest School of Medicine,
United States

Reviewed by:
Thomas J. Martin,
Wake Forest School of Medicine,
United States
Stephan Kellenberger,
University of Lausanne, Switzerland

***Correspondence:**
Ping Chen
chenp@hunnu.edu.cn
Songping Liang
liangsp@hunnu.edu.cn
Zhonghua Liu
liuzh@hunnu.edu.cn

[†] These authors have contributed equally to this work.

Specialty section:
This article was submitted to Neuropharmacology, a section of the journal Frontiers in Pharmacology

Received: 19 September 2017
Accepted: 07 November 2017
Published: 22 November 2017

Citation:
Zhou X, Xiao Z, Xu Y, Zhang Y, Tang D, Wu X, Tang C, Chen M, Shi X, Chen P, Liang S and Liu Z (2017) Electrophysiological and Pharmacological Analyses of $Na_V1.9$ Voltage-Gated Sodium Channel by Establishing a Heterologous Expression System. Front. Pharmacol. 8:852. doi: 10.3389/fphar.2017.00852

Na_V1. 9 voltage-gated sodium channel is preferentially expressed in peripheral nociceptive neurons. Recent progresses have proved its role in pain sensation, but our understanding of $Na_V1.9$, in general, has lagged behind because of limitations in heterologous expression in mammal cells. In this work, functional expression of human $Na_V1.9$ ($hNa_V1.9$) was achieved by fusing GFP to the C-terminal of $hNa_V1.9$ in ND7/23 cells, which has been proved to be a reliable method to the electrophysiological and pharmacological studies of $hNa_V1.9$. By using the $hNa_V1.9$ expression system, we investigated the electrophysiological properties of four mutations of $hNa_V1.9$ (K419N, A582T, A842P, and F1689L), whose electrophysiological functions have not been determined yet. The four mutations significantly caused positive shift of the steady-state fast inactivation and therefore increased $hNa_V1.9$ activity, consistent with the phenotype of painful peripheral neuropathy. Meanwhile, the effects of inflammatory mediators on $hNa_V1.9$ were also investigated. Impressively, histamine was found for the first time to enhance $hNa_V1.9$ activity, indicating its vital role in $hNa_V1.9$ modulating inflammatory pain. Taken together, our research provided a useful platform for $hNa_V1.9$ studies and new insight into mechanism of $hNa_V1.9$ linking to pain.

Keywords: electrophysiology, pharmacology, sodium channel, $Na_V1.9$, $Na_V1.9$ mutants, histamine

INTRODUCTION

Voltage-gated sodium channels (VGSCs) are a cluster of important transmembrane proteins, that play crucial roles for initiation and propagation of action potential (AP) in excitable tissues, including heart, brain and peripheral nerves (Catterall, 2000, 2012). All VGSCs are composed of a pore-forming α-subunit and one/two auxiliary β-subunits. To date, nine α-subunits ($Na_V1.1$-1.9, also referred as channels) and four β-subunits (β1-β4) have been identified in mammals (Bant and Raman, 2010; Catterall, 2014, 2015). Of the nine VGSC isoforms, $Na_V1.9$ is preferentially expressed

in peripheral nociceptive neurons, as well as visceral afferents (Padilla et al., 2007; Hockley et al., 2014; Dib-Hajj et al., 2015). It exhibits unique biophysical properties that include activation near resting membrane potential, slow activation and inactivation kinetics, generation of large persistent currents in low depolarizing voltages and large window current (Cummins et al., 1999; Dib-Hajj et al., 2002, 2015). These make $Na_v1.9$ act as a threshold channel in AP firing, amplifying sub-threshold stimulus that leads to AP burst and increases repetitive firing (Herzog et al., 2001; Dib-Hajj et al., 2002, 2015).

Preclinical studies in pain animal models suggest that $Na_v1.9$ might be involved in pain-signaling pathway (Lolignier et al., 2011, 2015; Hockley et al., 2014). Using $Na_v1.9$ null or knock down rodent models, it has been proved that $Na_v1.9$ contributes to regulating the excitability of sensory neurons (e.g., dorsal root ganglion (DRG) neurons) and plays a crucial role in inflammation-induced hyperalgesia (Baker et al., 2003; Ostman et al., 2008). More recently, genetic and functional findings illustrate that $hNa_v1.9$ mutations cause human pain diseases, which provides directly clinical evidences linking $hNa_v1.9$ to human pain. To date, a total of 16 mutations of $hNa_v1.9$ have been identified in individuals with rare genetic pain disorders and a population of patients with painful peripheral neuropathy (Leipold et al., 2013, 2015; Zhang et al., 2013; Huang et al., 2014, 2017; Han et al., 2015, 2017; Okuda et al., 2016; Phatarakijnirund et al., 2016). Patch-clamp analysis revealed that these are gain-of-function mutations, which are expected to correlate with the clinical phenotype of increased sensitivity to pain (Leipold et al., 2013, 2015; Zhang et al., 2013; Huang et al., 2014; Han et al., 2015). However, two mutations, L811P and L1302F, are associated with congenital insensitivity to pain, a phenotype contrary to functional evidences (Leipold et al., 2013; Woods et al., 2015; Huang et al., 2017). Huang et al. suggested that L811P and L1302F evoked large depolarization of resting membrane potential and impaired action potential generation (Huang et al., 2017). Therefore, all these studies validate the direct correlation between $hNa_v1.9$ and human pain.

Studies have proved that inflammatory mediators released from injured and inflammatory cells modulate $Na_v1.9$ currents to maintain inflammation-induced hyperalgesia (Baker et al., 2003; Priest et al., 2005; Amaya et al., 2006; Ostman et al., 2008), which probably supports a role for $Na_v1.9$ in inflammatory and neuropathic pain. Treatment of rat DRG neurons with prostaglandin E2 (PGE_2) was found to increase the amplitude of $Na_v1.9$ current (Rush and Waxman, 2004). Maingret et al. has indicated that $Na_v1.9$ is up-regulated by the concerted action of inflammatory soup, a well-defined mixture of histamine, PGE_2, bradykinin (BK), norepinephrine and ATP. Increased $hNa_v1.9$ current may contribute to lowering the threshold for AP firing and therefore render nociceptor hyperexcitable during peripheral inflammation (Maingret et al., 2008). It is worth noting that these results are based on acute isolation of rodent DRG neurons and inevitably affected by other VGSC subtypes expressed in the same neurons. Interestingly, anti-inflammatory medication reduces the frequency of painful events caused by $Na_v1.9$ mutation (Zhang et al., 2013; Leipold et al., 2015), which is consistent with the effects of inflammatory mediators.

Although, considerable progress has been made in recent years, our understanding of $Na_v1.9$ in general, has lagged behind. One of the primary reasons is that, it is difficult to study $Na_v1.9$ in heterologous expression systems, since it is only expressed at low levels and is hard to study in isolation in native neurons (Dib-Hajj et al., 2015; Goral et al., 2015; Lin et al., 2016). Meanwhile, the above findings have raised some questions. Even for the same $Na_v1.9$ mutations, studies in human mutant channel expressed in ND7/23 cells and in mouse mutant channel in DRG neurons have brought to striking differences in gating profiles because of specific sequence divergence, cell types used for channel expression or different recording protocols. In addition, the functions of five mutant channels have not been explored yet. The precise effect of inflammatory mediators on $hNa_v1.9$ and the underlying mechanisms needed to be investigated further. Generally speaking, a heterologous system expressing high level and stable $Na_v1.9$ current is still valuable; intensive electrophysiological analyses by using this heterologous expression system may contribute in part to answering these questions.

In the following study, we succeeded in achieving a functional expression of $hNa_v1.9$ channel in heterologous cells by fusing GFP to the C-terminal of $hNa_v1.9$ sequence, which provides a powerful platform for the electrophysiological studies of $hNa_v1.9$. Here, by applying this expression system, we systematically investigated the biophysical characteristics of wild type (WT) and mutant $hNa_v1.9$ channels, as well as elucidated the effects and mechanisms of inflammatory mediators on $hNa_v1.9$. This heterologous expression system of $hNa_v1.9$ is useful for the electrophysiological and pharmacological studies of this channel.

MATERIALS AND METHODS

Plasmid Constructs and Mutagenesis

The deleted stop codon cDNA of $hNa_v1.9$, using KpnI and SmaI enzyme site, was subcloned into the pEGFP-N1 vector (Clontech). Mutations were constructed by using the Quick-change II XL Site-directed Mutagenesis kit (Agilent Technologies) according to the manufacturer's instruction. All mutations were verified by DNA sequencing.

Cell Culture and Transfection

ND7/23 and HEK293T cells were maintained in Dulbecco's modified Eagle's medium (DMEM) supplemented with 10% fetal bovine serum, 2 mM L-glutamine, 100 U/ml penicillin and 100 μg/ml streptomycin in a 5% CO_2 incubator at 37°C; CHO-K1 cells were maintained in 45% DMEM and 45% F12K supplemented with 10% fetal bovine serum, 2 mM L-glutamine, 100 U/ml penicillin and 100 μg/ml streptomycin in a 5% CO_2 incubator at 37°C. Cells were trypsinized, diluted with culture medium, and grown in 35 mm dishes. When grown to 90% confluence, cells were transfected with $hNa_v1.9$-GFP or $hNa_v1.9$-GFP mutations using the transfection kit X-treme GENE HP DNA Transfection Reagent (Roche, Basel, Switzerland) according to the manufacturer's instructions (4 μg $hNa_v1.9$-GFP or $hNa_v1.9$-GFP mutant plasmid and 8 μl X-tree GENE HP DNA). Transfected cells were first maintained at 37°C

for 24 h, with 5% CO_2 and then incubated at 29°C with 5% CO_2 for 20 h, before use in electrophysiology experiments. The green fluorescent was used for visual identification of individual transfected cells.

Electrophysiology

Extracellular solution contained (in mM) 150 NaCl, 2 KCl, 1.5 $CaCl_2$, 1 $MgCl_2$, 10 HEPES (pH 7.4 with NaOH) and was supplemented with 1 μM tetrodotoxin (TTX) to block endogenous Na^+ currents in ND7/23 cells; the pipette solution contained (in mM) 35 NaCl, 105 CsF, 10 EGTA, 10 HEPES (pH 7.3 with CsOH). All salts were obtained from Sigma. Whole-cell voltage-clamp recordings were performed at room temperature (25 ± 2°C) using an EPC-10 USB patch-clamp amplifier operated by PatchMaster software (HEKA Elektronik, Lambrecht, Germany). Fire-polished electrodes (2.0–2.5 MΩ) were fabricated from 1.5-mm capillary glass using a P-97 puller (Sutter, Novato, CA). Capacity transients were canceled; voltage errors were minimized with 80% series resistance compensation. The liquid junction potential between the pipette and bath solutions was zeroed before seal formation. Voltage dependent currents were acquired with Patchmaster at 5-min after establishing whole-cell configuration, sampled at 30 kHz, and filtered at 2.9 kHz.

To generate activation curves, cells were held at −120 mV and stepped to potentials of −100 to +50 mV in 5-mV or 10-mV increments for 50-ms every 5-s. The G-V curves were obtained by calculating the conductance (G) at each voltage (V) using the equation $G=I/(V-V_{rev})$, with V_{rev} being the reversal potential determined for each cell individually. G-V curves were fitted using a Boltzmann equation: $y = 1/ (1 + exp[(V_a - V)/\kappa])$ in which V_a, V, and κ represented midpoint voltage of kinetics, test potential and slope factor, respectively. The repetition interval was 5-s.

Voltage dependent steady-state fast inactivation was measured with a series of 1,000-ms pre-pulses (−120 to 0 mV in 10-mV increments), followed by a 50-ms depolarization to −40 mV to assess the available non-inactivated currents, and the repetition interval was 10-s. Steady-state slow-inactivation was determined with 30 s pre-pulses ranging from −120 to −40 mV followed by a 100 ms pulse to −100 mV to remove fast-inactivation. Remaining available channels were activated by a 50 ms test pulse to −40 mV. The repetition interval was 40-s. Peak inward currents at the test pulse were normalized to the maximal inward current and fit with Boltzmann functions: $I / Imax = A + (1 - A) / \{1 + exp[(V - V_h) / \kappa]\}$, where V represents the inactivating pre-pulse potential, V_h is the midpoint of the steady-state fast-inactivation or slow-inactivation, A is the minimal channel availability, and κ is the slope factor.

The ramp current was measured by a small slow ramp depolarization protocol, which started from the holding potential of −100 mV and steadily increased to 20 mV over 600-ms at the rate of 0.2 mV/ms. The repetition interval was 10-s.

The deactivation current of each channel was measured using a 25-ms depolarization to −40 mV, followed by a 100-ms repolarizing pulse to potentials ranging from −120 to −80 mV in steps of 5-mV with a repetition interval of 10-s. The deactivation currents were fitted with a single exponential function according to: $I(t) = I_0 - (I_0 - I_\infty) \times (1 - e^{-t/\tau_d})$, where I_0 is the maximal current amplitude, $I_\infty$is the current remaining after infinite time, t is the time and τ_d is the deactivation time constant.

Dose response curves of histamine were fitted using the following Hill logistic equation: $y = f_{max} - (f_{max} - f_{min})/(1 + (x/EC_{50})^n)$, where f_{max} and f_{min} represent the maximum and minimum response of channel to histamine, the f_{min} was set to 0, x represents histamine concentration and n is an empirical Hill coefficient.

Drug Treatment

One micromolar TTX were applied in all experiments except special description. In measurements examining the effects of histamine receptor inhibitors on the histamine-enhanced $hNa_v1.9$ current, the ND7/23 cells expressing $hNa_v1.9$-GFP were pretreated for 30 min with 50 nM mepyramine (Abcam), 100 μM ranitidine (Abcam) or 1 μM thioperamide (Abcam), and they were also present when histamine was applied.

For electrophysiology experiments, the stock solution of drugs was diluted with fresh bath solution to a concentration of 10-fold of the interested concentration, 30 μl of the concentrated drugs was diluted into the recording chamber (containing 270 μl bath solution) far from the recording pipet (the recording cell) and was mixed by repeatedly pipetting to achieve the specified final concentration.

All compounds were dissolved in DMSO (TTX and PGE_2) or water (histamine, BK, 5-HT, mepyramine, ranitidine and thioperamide) to make 1 mM-1 M stock solutions. The final concentration of DMSO did not exceed 0.2%, which was found to have no significant effect on sodium currents.

Data Analysis

Data were analyzed with Fit-Master (HEKA Elektronik), Igor-Pro (WaveMetrics, Lake Oswego, OR, USA) software and Prism 5 (GraphPad Software). Data are presented as mean ± S.E.M, and n is presented as the number of the separate experimental cells. Statistical significance was assessed with GraphPad Prism using the paired Student's t-test or one-way ANOVA with Tukey's Multiple Comparison Test. Statistical significance was accepted at $P < 0.05$.

RESULTS

Functional Expression and Characterization of $hNa_v1.9$ Channel in Heterologous Cells

It has been a challenge for the functional expression of $Na_v1.9$ in heterologous cells such as HEK293T, CHO-K1, ND7/23, and Xenopus oocytes. ND7/23 cells are hybrids of neuro-blastoma and dorsal root ganglia cells. It was confirmed that >97% of macroscopic Na_v currents in ND7-23 cells is carried by TTX-sensitive channels (Zhou et al., 2003; Rogers et al., 2016). As shown in **Figures S1A,B**, the endogenous currents of ND7/23 cells were completely blocked by 200 nM TTX. Recently, Vanoye et al. found that functional expression of $Na_v1.9$ was achieved in ND7/23 cells when cells were cultivated at lower temperature

after transient transfection although the yield was rather poor (Vanoye et al., 2013). As shown in **Figure 1A**, ND7/23 cells were cultivated at 29°C after the transient transfection of $hNa_v1.9$-encoding DNA. The $Na_v1.9$ currents, in the presence of 1 μM tetrodotoxin (TTX), were distinctly recorded at 50-ms depolarizing steps with 10-mV increments from the holding potential of −120 mV. However, the peak current density was only −5.74 ± 1.44 pA/pF ($n = 6$) at the depolarizing voltage of −40 mV (**Figure 1B**), which is too small to functional analysis. Goral et al. showed that a chimera of $hNa_v1.9$ harboring the C-terminal of $rNa_v1.4$ yielded big currents in heterologous cells (Goral et al., 2015). Yet, the gating properties of activation and inactivation of the chimera channel were significantly different from those of WT-$hNa_v1.9$. It is not an optimal method to study $Na_v1.9$ gating and functions of mutant channels. In an attempt to studying the expression and translocation of $hNa_v1.9$, we linked GFP to the C-terminal of $hNa_v1.9$ sequence to construct a fusion protein channel ($hNa_v1.9$-GFP). After transfection in ND7/23 cells, this channel mediated large currents activated by a serial of 50-ms depolarizing pulses (ranging from −100 mV to 40 mV with 5-mV increments) from the holding potential of −120 mV in the presence of 1 μM TTX which completely blocked TTX-S currents in ND7/23 cells (**Figure 1A**). The current density was −34.21 ± 8.83 pA/pF ($n = 6$) at the depolarizing voltage of −40 mV when cells were cultivated at 37°C after transient transfection (**Figure 1B**); lower temperature culture (29°C) also enhanced the current density to −80.23 ± 8.4 pA/pF ($n = 12$) (**Figure 1B**), which is consistent with its role in the perception of cold pain under normal and pathological conditions (Leipold et al., 2015; Lolignier et al., 2015). From the current-voltage (I-V) curves as shown in **Figure 1C**, the fusion of GFP to $hNa_v1.9$ and lower temperature culture did not alter I-V curve shape and the voltage-dependence of activation. Namely, the initial activation voltage (∼-70 mV), the maximum activation voltage (∼-40 mV) and the reversal potential of $hNa_v1.9$ current in ND7/23 cells (∼35 mV) were not changed. The current was singularly stable, because the current amplitude showed no obvious alteration within 10 min recording (**Figure 1D**). In addition, the $hNa_v1.9$-GFP channel also had functional expression in HEK 293T and CHO-K1 cells, and both yielded current signals typical for $Na_v1.9$ channel (**Figures 1E–G**). Note that the currents in ND7/23 cells expressing $hNa_v1.9$-GFP channels could not affected by MrVIB that is a known blocker of $Na_v1.8$ (MrVIB/Control = 0.99 ± 0.01, $n = 3$) but not $Na_v1.9$, indicating that these currents were actually mediated by $hNa_v1.9$ without being mixed by $Na_v1.8$ (**Figure 1H**; Ekberg et al., 2006). Because of larger currents observed and the DRG background of ND7/23 cells which contains accessory Na^+ channel β1and β3 subunits (Rogers et al., 2016), our studies were performed in this cell line.

After establishing a dependable heterologous expression of $hNa_v1.9$, we proceeded with determining more detailed biophysical properties of this channel. As shown in **Figure 1A**, representative voltage-dependent inward currents of $hNa_v1.9$ exhibited slow activation and inactivation at low potentials. The voltage-dependence of activation and steady-state fast inactivation for $hNa_v1.9$ generated a large overlap (window current) (**Figure 2A**), and the midpoints of activation (V_a) and steady-state fast inactivation (V_h) were −53.3 ± 0.9 and −69.4 ± 0.7 mV (**Table 1**), respectively. The steady-state slow-inactivation, a process that inactivates the channel much more slowly than fast-inactivation, had the midpoint value of −77.1 ± 0.8 mV (**Figure 2A** and **Table 1**). We also measured the recovery from inactivation (repriming) of $hNa_v1.9$ after a 50-ms depolarization to −40 mV and found it exhibited fast priming, and the time constant was 13.7 ± 0.7 ms (**Figure 2B**). The protocol was shown in **Figure 2Ca**. These data were consistent with previous results of WT-$Na_v1.9$ currents observed in DRG neurons or ND7/23 cells (see **Table 1**).

Inactivation is an intrinsic property for VGSCs. There are two kinds of inactivation. Open-state inactivation (OSI) may occur from the open state at strongly depolarized membrane potentials, while closed-state inactivation (CSI) may be generated from pre-open closed states at hyperpolarized membrane potentials (Armstrong, 2006; Bähring and Covarrubias, 2011). The OSI of $Na_v1.9$ is extremely slow, generating persistent current. Nevertheless, the CSI of $Na_v1.9$ still maintains unkown. In this work, we investigated for the first time the development of CSI of $hNa_v1.9$ using a standard development of inactivation voltage protocol (**Figure 2Cb**). As shown in **Figure 2B**, it displayed a slow rate for the development of CSI, where only 18% current was inactivated at a 1,024-ms pre-pulse at −100 mV. The slow rate for CSI development indicated that the transition from the closed state to closed-inactivated state is slow for $hNa_v1.9$. Consequently, the channel is less-likely to undergo closed-state inactivation during slow depolarization. Cummins et al. proposed that slow development of CSI contributes to the generation of large ramp current in VGSCs (Cummins et al., 1998). Indeed, a large ramp current of $hNa_v1.9$ in ND7/23 cells was elicited in response to slow ramp depolarization (0.2 mV/ms), which was 32.2 ± 1.0% ($n = 16$) of the peak transient current of the same cells. The voltage at which the peak of the ramp current was produced was −51.9 ± 1.1 mV ($n = 16$) (**Figure 2D** and **Table 2**). These data prompted that $hNa_v1.9$ has capability to open at voltages close to membrane potential. Our study provided more solid evidences to support that $Na_v1.9$ serves as a subthreshold amplifier.

Functional Analysis of $hNa_v1.9$ Mutations by the $hNa_v1.9$-GFP Heterologous Expression System

Of the 16 mutations of $hNa_v1.9$ causing human pain disorders, five mutations (K419N, A582T, A681D, A842P, and F1689L, their location in the $Na_v1.9$ sequence are shown in **Figure 3A**) associated with painful peripheral neuropathy were not functionally analyzed (Huang et al., 2014). We measured the biophysical characteristics of four mutants in ND7/23 cells (of the five mutants, A681D was not functionally expressed in ND7/23 cells). As shown in **Figure 3**, all the four mutants (K419N, A582T, A842P, and F1689L) positively shifted the steady-state fast inactivation significantly and had no obvious effect on activation, resulting in larger window currents (**Figures 3B–E**); they did not change the deactivation time significantly, compared with the WT-channel (**Figure 3F**); except F1689L, the other three mutations had augmented ramp currents (**Figure 3G**). Quantified biophysical parameters for

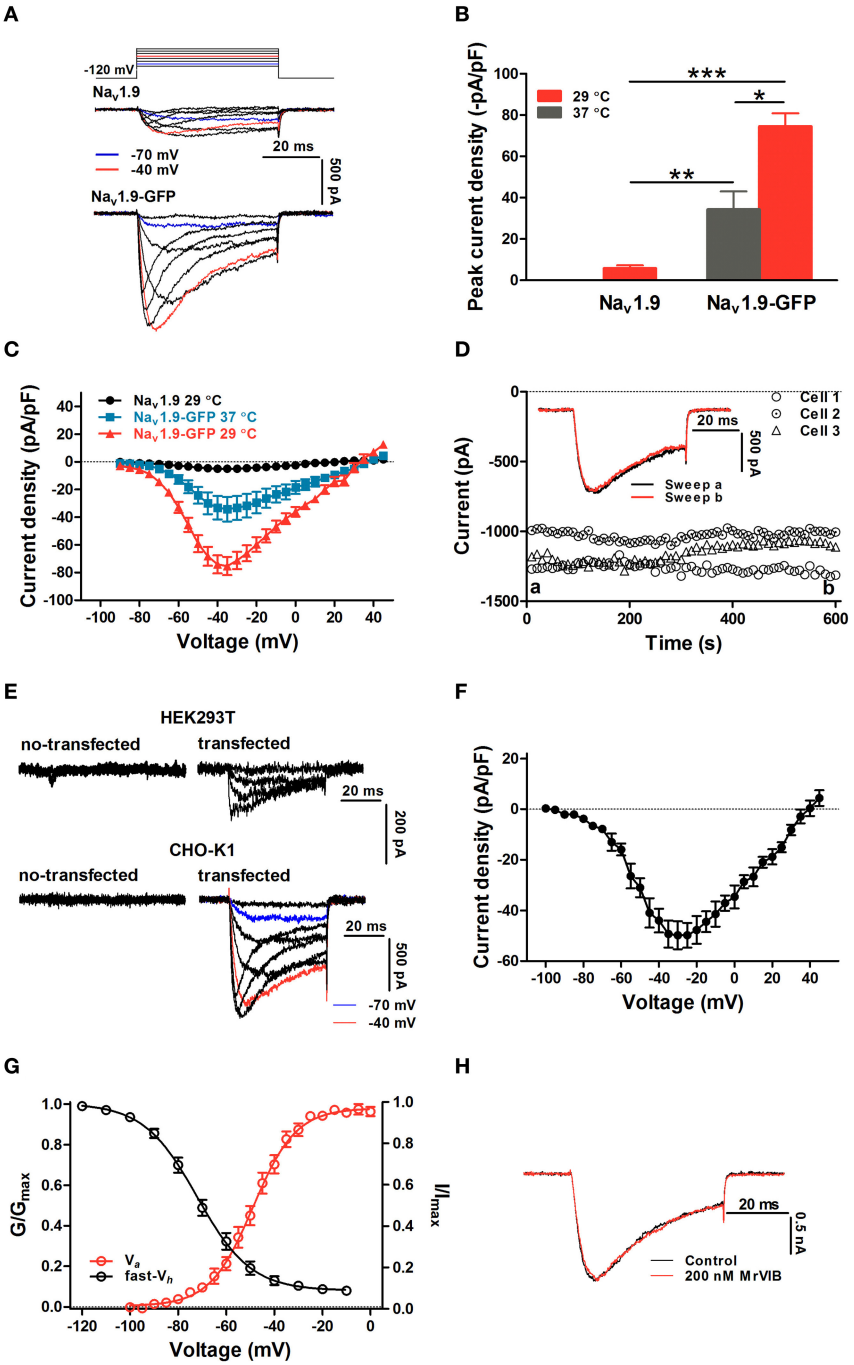

FIGURE 1 | Functional expression and characterization of hNa$_V$1.9 in heterologous cells. **(A)** Representative inward currents of hNa$_V$1.9 or hNa$_V$1.9-GFP transiently transfected in ND7/23 cells cultivated at 29°C. Currents were evoked by depolarization from a holding potential of −120 mV up to −10 mV in 10-mV steps. Note that the data were recorded 5 min after establishing whole-cell configuration. **(B)** Comparison of peak current densities of hNa$_V$1.9 and hNa$_V$1.9-GFP in ND7/23 cells cultivated at 37° or 29°C. *$p < 0.05$; **$p < 0.01$; ***$p < 0.001$. **(C)** Current-voltage relationships measured from channels indicated. **(D)** The stability of hNa$_V$1.9-GFP current in ND7/23 cells that elicited by a 50-ms depolarization to −50 mV from a holding potential of −120 mV. Data sweeps were acquired at 0.1 Hz. The *inset* shows representative current traces before (sweep a) and after (sweep b) a 10-min recording. **(E)** Representative current traces in HEK 293T (*upper*) or CHO-K1 (*below*) cells transfected with hNa$_V$1.9-GFP. Currents were activated by depolarizing up to −10 mV in 10-mV steps from a holding potential of −120 mV. **(F)** Current density-voltage relationship of hNa$_V$1.9 in CHO-K1 cells. The cells were held at −120 mV and stepped to potentials of −100 to +40 mV in 5-mV increments for 50-ms every 5-s. **(G)** The steady state activation and inactivation of hNa$_V$1.9 in CHO-K1 cells. Data points were well fitted with the Boltzmann equation. Voltage-dependent activation was derived from the data in **(F)**. Voltage-dependent steady-state fast inactivation of hNa$_V$1.9 in CHO-K1 cells was measured with a series of 1,000-ms prepulse (−120 to −10 mV in 10-mV increments), followed by a 50-ms depolarization to −40 mV to assess the available non-inactivated channels. **(H)** During pre-incubated with MrVIB 2 min, MrVIB had no effect on the hNa$_V$1.9-GFP current in ND7/23 cells. The current was activated by a 50-ms depolarization of −40 mV from the holding potential of −120 mV. 1 μM TTX were applied in all experiments.

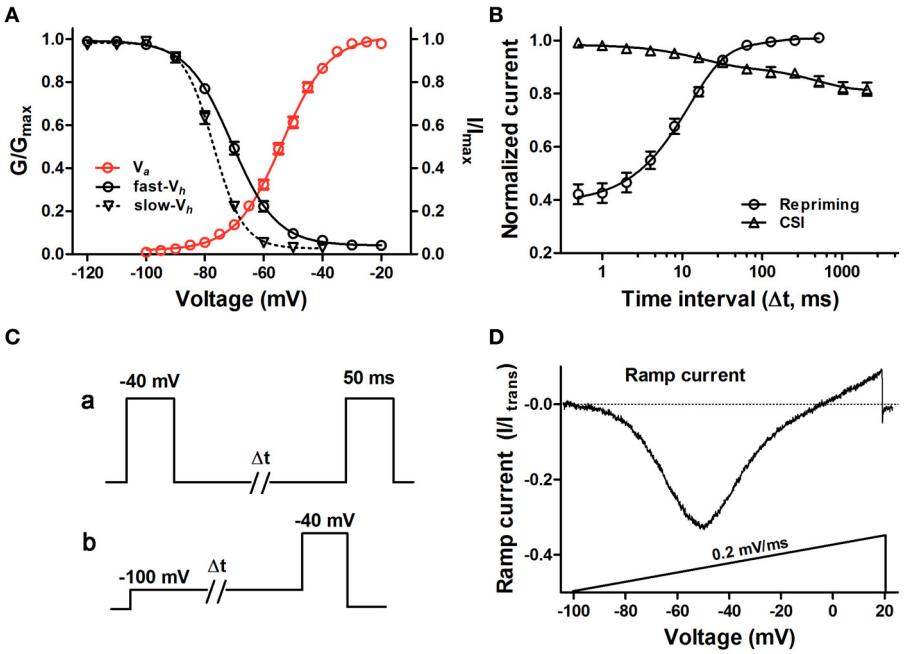

FIGURE 2 | Biophysical properties of $hNa_v1.9$-GFP in ND7/23 cells. **(A)** Voltage-dependent activation, steady-state fast-inactivation and slow-inactivation of $hNa_v1.9$-GFP. Data points for activation and inactivation kinetics were well fitted with the Boltzmann equation. **(B)** Time course of recovery from fast inactivation and development of close-stated inactivation of $hNa_v1.9$-GFP. Lines represent data fitted with a one-exponential function. **(C)** Protocols for the recovery from fast inactivation **(a)** and the development of CSI **(b)**. To determine the recovery from fast inactivation, a 50-ms prepulse at −40 mV was used to move channels into the fast inactivated state, followed by a pulse at −120 mV with increased duration to allow channels to recover from fast inactivation before a 50-ms test pulse at −40 mV to measure the available current. To determine the development of CSI, from a holding potential of −120 mV, the cells were prepulsed to −100 mV (pre-open state) for increasing durations before a 50-ms test pulse to −40 mV. The repetition interval was 10-s. **(D)** Representative ramp currents of $hNa_v1.9$-GFP in response to slow depolarization (0.2 mV/ms) were normalized to the transient peak current and plotted as a function of membrane potentials. Data points are represented as mean ± S.E.M. One micro molar TTX were applied in all experiments.

these channels are provided in **Table 2**. These data implied that the four mutations might enhance $hNa_v1.9$ activity and cause increased sensitivity to pain.

Histamine Enhances $hNa_v1.9$ Activity

Previous studies have shown that some pro-inflammatory mediators potentiate $Na_v1.9$ activity, resulting in enhanced nociceptor excitability (Maingret et al., 2008). In the present study, the effects of inflammatory mediators, including histamine, bradykinin (BK), PGE_2, and 5-TH, were elucidated by using the $hNa_v1.9$-GFP heterologous expression system. First of all, we found histamine directly enhanced $hNa_v1.9$ current, which has not been reported in previous studies. As show in **Figure 4A**, adding 1 mM histamine to bath solution potently increased $Na_v1.9$ current in ND7/23 cells by 37.9 ± 6.3% ($n = 6$). **Figure 4B** shows the time course of the action of histamine at different concentrations. In contrast to 0.1 and 0.5 mM histamine, 1 mM histamine showed a rapid onset of action. Within 5 s, the action could reach the maximum and maintain stable. The action of histamine is reversible, since the peak current would rapidly return back to control level upon washing (**Figures 4A,B**). There are endogenous TTX-S Na^+ currents in ND7/23 cells we used and it was reported that histamine also strengthened the activation of TTX-S Na^+ currents (**Figure S1C**). Although no detectable TTX-S Na^+ currents in ND7/23 cells were elicited at lower depolarized voltages (e.g., −50 mV), as show in **Figure S2A**, we still used CHO-K1 cells (no detectable endogenous TTX-S currents were examined) for the functional expression of $hNa_v1.9$-GFP. Significant enhancement of $hNa_v1.9$ peak current was observed in the presence of 1 mM histamine, while in control cells, no obvious currents was induced by histamine (**Figure S2A**). In contrast to histamine, 1 mM 5-TH (5-TH/Control = 1.0 ± 0.01, $n = 4$, $P > 0.05$), 100 μM BK (BK/Control = 1.0 ± 0.01, $n = 3$) and 100 μM PGE_2 (PGE_2/Control = 0.99 ± 0.01, $n = 5$) did not affect $hNa_v1.9$ current when they were added directly to bath solution (**Figure S2F**). These data confirmed the action of histamine on $hNa_v1.9$.

The action of histamine was dose-dependent and voltage-dependent. Higher concentrations of histamine led to greater enhancement of $hNa_v1.9$ current (**Figure 4C**). However, the enhancement of $hNa_v1.9$ current by histamine was negatively correlated with depolarization voltages. For example, compared with control, 10 mM histamine treatment resulted in 25.3 ± 4.2, 161.8 ± 20.5, and 285.4 ± 5.0% ($n = 3$) of increments of $hNa_v1.9$ currents at −30, −50 and −70 mV, respectively. This was also observed in I-V curves (**Figure 4D**). In the presence of 1 mM histamine, larger currents occurred at lower depolarization

TABLE 1 | Biophysical properties of this paper and previous studies of $Na_V1.9$ channels.

References	Cell type	Current density (pA/pF)	Voltage dependence of activation (mV)		Steady-state fast inactivation (mV)		Steady-state slow inactivation (mV)	
			V_s	*K*	Fast-V_h	*K*	Slow-V_h	*K*
This study	ND723	−80.23±8.4	−53.3±0.9 ($Na_V1.9$-GFP 29°C)	7.6 ± 0.2	−67.6 ± 1.2	7.2 ± 0.4	−77.1 ± 0.8	5.2 ± 0.3
		−5.74 ± 1.44	−51.8 ± 1.9 ($Na_V1.9$ 29°C)	6.8 ± 0.3	N		N	
		−34.21 ± 8.83	−54.8 ± 2.9 ($Na_V1.9$-GFP 37°C)	7.0 ± 0.2	N		N	
	CHO-K1	−49.8 ± 7.6	−47.7 ± 1.9 ($Na_V1.9$-GFP 29°C)	8.4 ± 0.3	−71.7 ± 2.2	10.7 ± 0.7	N	
Leipold et al., 2015	ND7/23	∼5.0	−52.0 ± 2.6 (30°C)	9.1 ± 0.7	−69.1 ± 3.9(30°C)	9.3 ± 1.2	N	
		∼5.0	−47.5 ± 2.5 (20°C)	10.1 ± 0.8	−71.5 ± 3.5(20°C)	10.0 ± 1.1	N	
Leipold et al., 2013	ND7/23	∼8	−51.6 ± 1.2	11.8 ± 0.8	−63.9 ± 0.6	8.9 ± 0.5	N	
	DRG (mNa,1.9)	∼250	−45.2 ± 8.0	7.7 ± 0.2	−74.7 ± 2.2	10.7 ± 2.2	N	
Vanoye et al., 2013	ND7/23	−37.4 ± 13.2	−56.9 ± 0.6	6.7 ± 0.3	−52.1 ± 2.6	9.2 ± 0.7	N	
Zhang et al., 2013	DRG	∼-90	−59.0 ± 0.7	5.1 ± 0.5	−57.3 ± 0.7	NR	N	
Huang et al., 2014	DRG	−135 ± 36	−49.6 ± 2.0	7.3 ± 0.5	−50.5 ± 1.3	10.7 ± 0.8	−79.0 ± 1.7	5.3 ± 0.1
		−231 ± 50	−55.3 ± 1.8	7.93 ± 0.61	−53.3 ± 1.7	10.6 ± 1.6	−81.9 ± 4.1	6.98 ± 0.92
Huang et al., 2017	DRG	−23.4 ± 2.2	−54.2 ± 1.3	7.1 ± 1.3	−55.3 ± 2.3	8.1 ± 0.5	N	
Han et al., 2015	SCW	−52±10	−50.0 ± 1.5	8.4 ± 0.3	−42.0 ± 1.1	10.3 ± 0.3	−73.6 ± 1.3	7.3 ± 0.2
Han et al., 2017	DRG	−74.5 ± 11.7	−47.5 ± 1.7	8.2 ± 0.4	−53.9 ± 2.3	10.1 ± 0.5	−82.9 ± 2.4	6.8 ± 0.3
Padilla et al., 2007	TG	N	−55.0 ± 2.0	6.2 ± 0.2	N		N	
	DRG	N	−58.0 ± 2.5	5.6 ± 0.3	N		N	
	Myenteric neurons	N	−53.0 ± 3.0	7.2 ± 0.3	N		N	

N, not reported; SCW, superior cervical ganglion; TG, trigeminal ganglion. In this study, these temperatures are cells incubation temperatures. In Leipold et al. (2015) study, these temperatures are recording temperatures.

TABLE 2 | Biophysical properties of the WT and mutant $hNa_V1.9$ channels.

$Na_V1.9$	Current density (pA/pF)	Activation (mV)			Steady-state of inactivation (mV)			Ramp current (0.2 mV/ms)		
		V_a	K	n	V_h	K	n	% of $I_{trans\ peak}$	V_{peak} (mV)	n
WT	−113.2 ± 14.3	−53.3 ± 0.9	7.6 ± 0.2	31	−69.4 ± 0.7	6.9 ± 0.3	13	32.2 ± 1.0	−51.9 ± 1.1	16
K419N	−151.9 ± 18.3	−53.8 ± 1.4	7.3 ± 0.3	15	−66.2 ± 1.1*	6.8 ± 0.3	9	36.8 ± 1.3*	−50.6 ± 1.5	24
A582T	−85.0 ± 12.2	−53.5 ± 1.8	7.9 ± 0.4	12	−64.7 ± 1.1***	7.3 ± 0.2	10	44.6 ± 1.6***	−46.4 ± 1.7*	25
A842P	−81.5 ± 11.6	−51.9 ± 0.7	7.5 ± 0.2	19	−65.4 ± 0.8**	6.9 ± 0.2	16	38.6 ± 1.1***	−48.8 ± 1.1	30
F1689L	−100.8 ± 12.6	−50.5 ± 1.3	7.5 ± 0.2	13	−65.9 ± 1.0**	7.2 ± 0.3	12	35.7 ± 2.1	−49.4 ± 1.1	24

*$p < 0.05$; **$p < 0.01$; ***$p < 0.001$.

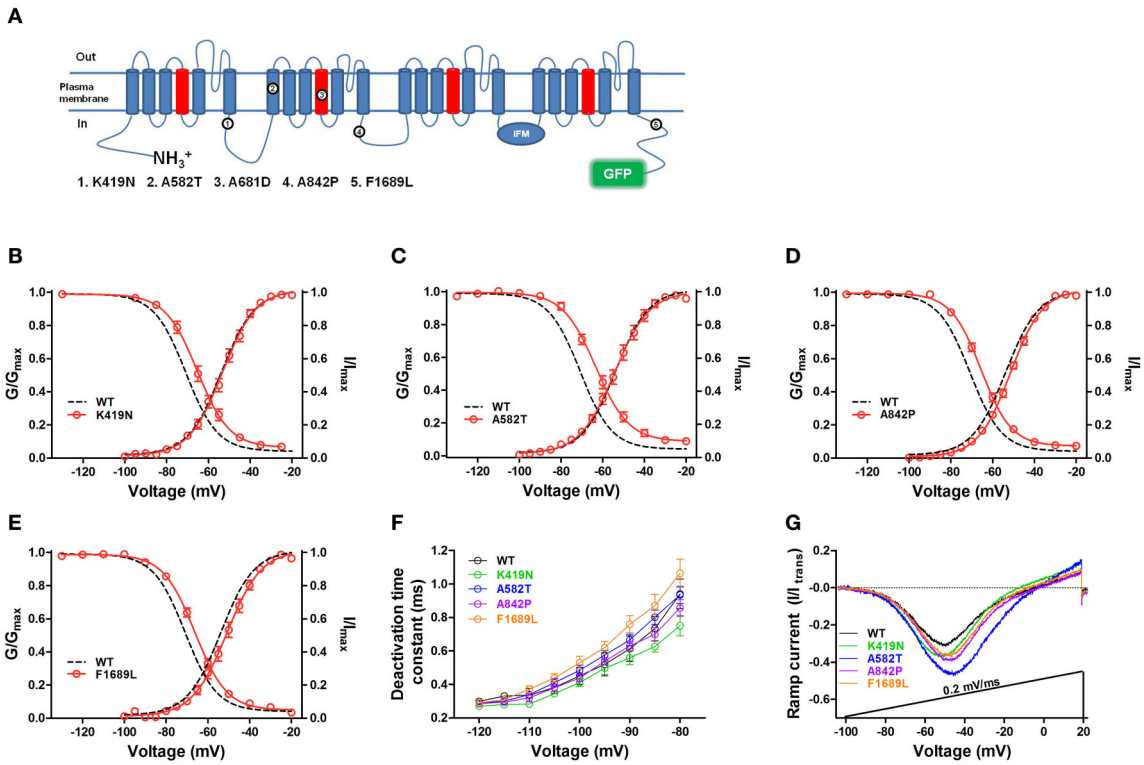

FIGURE 3 | Functional analysis of $hNa_V1.9$ mutations by the $hNa_V1.9$-GFP heterologous expression system. **(A)** Membrane topology of $Na_V1.9$-GFP with the position of mutants. Hollowed circles (numbered 1–6) represent amino acid substitutions in hNaV1.9 from individuals with pain disorders. Four mutant channels were functionally expressed in ND7/23 cells. Compared with WT-$hNa_V1.9$, the steady-state fast inactivation of the K419N **(B)**, A582T **(C)**, A842P **(D)**, and F1689L **(E)** mutants were significantly shifted in depolarization direction, but no obvious change of the voltage dependent activation was noticed. **(F)** The time courses of deactivation of the mutants were not significantly different from that of the WT-channel. **(G)** Representative ramp currents of the four mutants in response to slow depolarization (0.2 mV/ms) were normalized to the corresponding peak current acquired during activation protocol and plotted as a function of membrane potentials. One micro molar TTX were applied in all experiments.

voltages, and significant enhancements of $hNa_V1.9$ current were observed between −70 and −40 mV. In addition, histamine had no effect on the reversal potential of $hNa_V1.9$ current (control: 33.3 ± 2.7 mV, histamine: 30.2 ± 3.5 mV, $n = 12$, $P > 0.05$).

Histamine (1 mM) significantly shifted $hNa_V1.9$ activation by −4.5 ± 0.7 mV (control: −49.3 ± 1.4 mV, histamine: −53.7 ± 1.9 mV, $n = 9$, $P < 0.001$, paired t-test), whereas it had no significant effect on the steady-state fast-inactivation (control: −67.1 ± 1.3 mV, histamine: −69.7 ± 1.3 mV, $n = 9$, $P > 0.05$, paired t-test) (**Figure 4E**). Consistent with the effect of histamine on the activation, the peak of the ramp current was significantly shifted by −4.1 ± 0.4 mV, ($n = 8$, $P < 0.001$, paired t-test), and the ramp current amplitude was also enhanced by 18.4 ± 2.1% ($n = 8$, $P < 0.001$, paired t-test) in the presence of 1 mM histamine (**Figure 4F**). These data indicated that histamine enhanced $hNa_V1.9$ current through promoting the channel activation.

In addition, we found that with the pretreatment of 50 nM mepyramine (selective H1 inverse agonist), 100 μM ranitidine (selective H2 antagonist) or 1 μM thioperamide

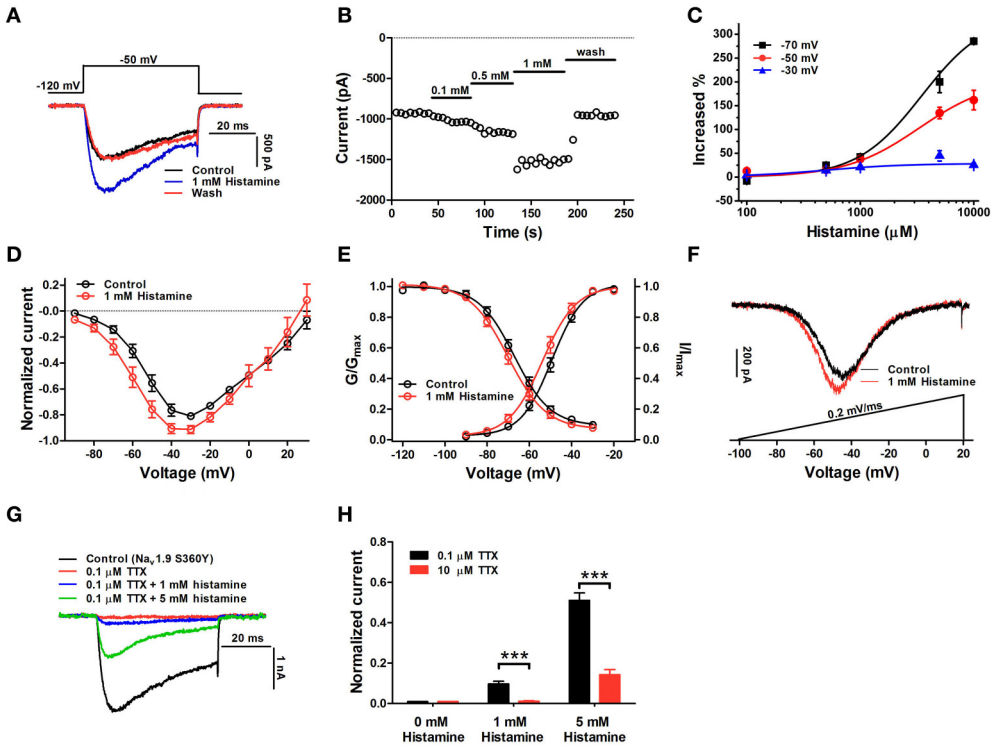

FIGURE 4 | Histamine enhances $hNa_V1.9$ activity in ND7/23 cells. **(A)** Current traces of a representative cell expressing $hNa_V1.9$ before and after application of 1 mM histamine and after washing with extracellular solution. **(B)** Time course of enhancement of $hNa_V1.9$ currents by histamine. The enhancement could be reversed by washing. **(C)** The dose- and voltage-dependent enhancement of histamine on $hNa_V1.9$ currents evoked by different depolarizing potentials (−30, −50, or −70 mV) from a holding potential of −120 mV. **(D)** The current-voltage curves indicate that 1 mM histamine changes the current-voltage relationship of $hNa_V1.9$. **(E)** 1 mM histamine significantly enhances the steady-state activation but not fast inactivation of $hNa_V1.9$. **(F)** Compared with control, 1 mM histamine enhances $hNa_V1.9$ ramp current and causes a hyperpolarized shift of the peak current. **(G)** Representative current traces show that 0.1 μM TTX completely block the current mediated by the S360Y $hNa_V1.9$ channel, which can be partially rescued by histamine. **(H)** Bars show when TTX concentration was raised to 10 μM, the recovery effect was significantly reduced for both 1 and 5 mM histamine. Data points are represented as mean ± S.E.M. ***$p < 0.001$. One micro molar TTX were applied in all experiments except special description.

(H3/H4 antagonist), the enhancement of $hNa_V1.9$ currents in ND7/23 cells by 1 mM histamine was not significantly different from that in the absence of these reagents (**Figure S2B**). Quantified data are provided in **Table 3**. Notably these inhibitors themselves had no effect on $hNa_V1.9$ current in ND7/23 cells (**Figures S2C–E**). These data demonstrate that histamine might increase $hNa_V1.9$ current independently of histamine receptors.

In our study, we found histamine was able to counteract TTX blockage on TTX-S Na^+ currents (**Figure S1C**). We therefore mutated the 360th serine of $hNa_V1.9$ to tyrosine, which makes this channel sensitive to TTX. In the presence of 0.1 μM TTX which completely block the current mediated by the S360Y mutant, the treatment of 1 or 5 mM histamine led to 14.2 ± 2.6% or 51.1 ± 3.7% recovery of currents triggered by a depolarization of −50 mV from a holding potential of −120 mV (**Figures 4G,H**). On the other hand, when TTX concentration was increased to 10 μM, the recovery effect was significantly reduced for both 1 and 5 mM histamine. These data implied that antagonistic effect might exist between TTX and histamine.

DISCUSSION

The $hNa_V1.9$-GFP Heterologous Expression System Provides a Promising Method for $hNa_V1.9$ Studies

VGSCs are essential for the initiation and propagation of AP in excitable tissues such as nerves and muscles. They also participate in many pathological processes and are targets of clinical drugs (Fozzard et al., 2005; Imbrici et al., 2016). Therefore, studies regarding to VGSCs have been attracted interests from scientific area and pharmaceutical industry. Functional expression of human VGSCs in heterologous cells is an important and widely-used method to their studies. Of the nine subtypes of VGSCs ($Na_V1.1$-1.9), except $Na_V1.9$, the other eight subtypes have been achieved functional expression in heterologous cells, such as HEK 293, CHO, ND7/23, and *Xenopus* oocytes. For $hNa_V1.9$, the only feasible method is to express it heterologous in DRG neurons of $Na_V1.9^{-/-}$ mice. However, expression of large plasmids in DRG neurons is discommodious and expensive because of the need to isolate and cultivate primary neurons. Furthermore, $Na_V1.8$ channels natively expressed in the neurons become the major

TABLE 3 | The effects of the inhibitors of the H1-4 receptors on the histamine-enhanced $hNa_v1.9$ current.

	−70 mV (%)	−60 mV (%)	*n*
Histamine	44.8 ± 3.8	39.5 ± 5.1	7
Histamine + Mepyramine	54.7 ± 14.6	41.9 ± 10.7	5
Histamine + Ranitidine	39.1 ± 5.6	30.0 ± 5.5	6
Histamine + Thioperamide	51.3 ± 2.3	41.4 ± 4.7	3

TTX-R background to compromise a faithful investigation of $Na_v1.9$ currents, which makes this method difficult to be used widely (Huang et al., 2014; Goral et al., 2015). Therefore, great efforts have been made to establish convenient and reproducible methods. Evidences indicate that low temperature culture of transfected cells and modification of the $Na_v1.9$ C-terminal are helpful for functional expression of $Na_v1.9$ (Vanoye et al., 2013; Goral et al., 2015), which inspires us to generate a fusion protein channel ($hNa_v1.9$-GFP). Compared with previous expression system, this $hNa_v1.9$-GFP heterologous expression system has advantages as follows. (1) It expresses large and stable current (>1 nA) in ND7/23 cells, which is essential to experimental data collection. (2) Compared with WT-$Na_v1.9$ in ND7/23 cells or DRG neurons (see **Table 1**), it shows similar properties with respect to the voltage dependence of activation and inactivation. (3) It is able to express functionally in different cell types, including ND7/23, HEK293T and CHO cells. In addition, it has advantages in convenience, high-efficiency, reproducibility and low-consumption, since the fused GFP serves as a fluorescent tracer and only one plasmid is used for transfection. Thus, with the $hNa_v1.9$-GFP heterologous expression system, we developed a feasible method suitable for $hNa_v1.9$ studies. For example, it helps to study the biophysical properties of $hNa_v1.9$ and functional analysis of clinical mutants. It is noted that more recently, a group from Pfizer Inc. established a $Na_v1.9$ stably expressed HEK 293 system by coexpression of $Na_v1.9$ with β1/β2 subunits (Lin et al., 2016), which was used for $Na_v1.9$ modulator screening. We are now constructing $hNa_v1.9$ stably expressed ND7/23 cell lines, which will be conveniently applied to high-throughput screening of therapeutic agents.

The Electrophysiological Mechanism Underlying the Gain of Function Mutations Causing Pain

The functions of four $hNa_v1.9$ mutant channels have been elucidated by using the $hNa_v1.9$-GFP heterologous expression system. We attempted to offer electrophysiological evidences linking mutant channel functions to phenotypes through a comparative analysis. Our data, together with those reported previously, show that these mutations result in depolarized shift of inactivation of $hNa_v1.9$, which therefore increases the open probability of $hNa_v1.9$ and leads to sensitivity to pain.

Histamine Directly Modulates the Activity of $hNa_v1.9$

Histamine is an important inflammatory mediator in pain processing and modulation. It can be released following mast cell degranulation by some inflammatory mediators including substance P, interleukin-1 and NGF (Dray, 1995; Woolf and Ma, 2007). In the peripheral nervous system, histamine directly sensitizes nociceptors and facilitates pain transmission, or indirectly causes pain via H1 receptors (Gorelova and Reiner, 1996; Mobarakeh et al., 2000; Kajihara et al., 2010; Yu et al., 2013). Histamine was discovered to upregulate $Na_v1.8$ expression via H2 receptor-mediated pathway, which might contribute to neuropathic pain (Vanoye et al., 2013; Yue et al., 2014). Recent studies indicate that histamine also has ionotropic receptors apart from metabotropic GPCRs H1-H4 (Haas and Panula, 2003). It directly activates ionotropic GABAA receptor β3 homooligomers and potentiates GABA responses in αβ heterooligomers via a site homologous to the GABA site in αβγ receptors (Saras et al., 2008; Thiel et al., 2015; Hoerbelt et al., 2016). It also selectively potentiates the response of ASIC1a homomers to acidification in CHO cells (Nagaeva et al., 2016). Interestingly, our results revealed that histamine positively modulates $hNa_v1.9$ activity by promoting channel activation and potentiates ramp current amplitude. These data expand our understanding for the function of histamine and mechanism of pain processing by histamine. In the present study, histamine has a lower affinity for $hNa_v1.9$ than the metabotropic histamine receptor, and the EC_{50} was 3.3 ± 0.5 mM at the depolarizing voltage of −50 mV. In spite of this, 0.5 mM histamine potently increased $hNa_v1.9$ current by ∼25% (**Figure 4C**). However, in inflammatory tissue, histamine concentrations could reach 1 mM at transient and local inflammatory area (Adams and Lichtenstein, 1979; Benbarek et al., 1999). Nevertheless, our finding provides clues for illuminating the mechanism of $hNa_v1.9$ in inflammatory and neuropathic pain. Our data also reveal that histamine could directly act on $hNa_v1.9$, which could be explained as follows: (1) The action of histamine on $hNa_v1.9$ displays rapid association and dissociation kinetics as revealed by the fast onset of action and recovery upon washing. This might rule out indirect modulations by histamine targeting other proteins which can regulate $hNa_v1.9$ activity through protein-protein interaction, posttranslational modification or transcriptional regulation, since these processes often take effect within extended period of time. (2) TTX and histamine had antagonistic effect on the S360Y $hNa_v1.9$ channel, which implied that they might possibly have partially overlapped binding site or the binding of histamine to $hNa_v1.9$ might likely alter the local structure of TTX binding site and then reduce TTX binding affinity to the S360Y channel. TTX is a known VGSC blocker by docking on extracellular pore of VGSCs (Penzotti et al., 1998). We speculate that the amino acid residues in pore region might possibly constitute the receptor of histamine in $hNa_v1.9$.

CONCLUSION

In conclusion, we have established a $hNa_v1.9$ heterologous expression system, which is effective and reliable for $hNa_v1.9$ studies. Using this system, we attempted to elucidate the electrophysiological mechanism of $hNa_v1.9$ in pain signaling and made new discoveries. The biophysical properties of $hNa_v1.9$ were systematically investigated in ND7/23 cells, which sheds new light on the role of $Na_v1.9$ as a threshold channel. Histamine can upregulate $hNa_v1.9$ activity through direct interaction,

expanding our understanding of the importance of $hNa_v1.9$ in inflammatory and neuropathic pain. Due to the complexity of physiological and pathological conditions, we do not expect with only electrophysiological data the mechanistic basis of $hNa_v1.9$ in pain signaling would be fully expounded. Undoubtedly, our study has given new insight into the electrophysiological mechanism underlying $hNa_v1.9$ involving in human pain sensation.

AUTHOR CONTRIBUTIONS

ZL, XZ, SL, PC, and XS designed all experiments. XZ performed all experiments and data analysis. ZX, YZ, and DT performed patch clamp analysis and plasmid construction and collection. YX and XW performed plasmid construction and collection. CT and MC helped to perform data analysis. ZL and XZ wrote the manuscript.

FUNDING

This work was supported by the National Science Foundation Projects (31370854, 31370817, 31370783, 31570782, and 31770832); the Science Found for Distinguished Young Scholars of Hunan Province (No. 14JJ1018); the Cooperative Innovation Center of Engineering and New Products for Developmental Biology of Hunan Province (No. 20134486).

ACKNOWLEDGMENTS

We thank Professor P. Alewood for generously and kindly providing MrVIB.

SUPPLEMENTARY MATERIAL

The Supplementary Material for this article can be found online at: https://www.frontiersin.org/articles/10.3389/fphar.2017.00852/full#supplementary-material

Figure S1. | (A) Representative current traces of ND7/23 cells expression of endogenous Na_V currents before and after the application of 200 nM TTX ($n = 5$). **(B)** I-V curves show that 200 nM TTX completely block the endogenous Na_V currents of the ND7/23 cells ($n = 5$). **(C)** I-V curves show when histamine concentration was raised to 10 mM, histamine was able to completely counteract TTX blockage on TTX-S Na^+ currents in ND7/23 cells ($n = 5$).

Figure S2. | (A) Representative current traces of CHO-K1 cells with or without expressing $hNa_V1.9$-GFP before and after the application of 1 mM histamine ($n = 3$). The current was activated by a 50-ms depolarization to −40 mV from a holding potential of −120 mV. **(B)** The effects of the inhibitors of the H1-4 receptors on the histamine-enhanced $hNa_V1.9$ current. The ND7/23 cells expressing $hNa_V1.9$, were pretreated for 30-min with 50 nM mepyramine (selective H1 inverse agonist, $n = 5$), 100 μM ranitidine (selective H2 antagonist, $n = 6$) or 1 μM thioperamide (H3/H4 antagonist). **(C–E)** H1-4 receptors inhibitors had no effect on $hNa_V1.9$ currents in ND7/23 cells ($n = 4$–7). **(F)** 5-TH (1 mM, $n = 4$), BK (100 μM, $n = 4$) or PGE_2 (100 μM, $n = 5$) did not affect $hNa_V1.9$ current when they were added directly to bath solution. Representative currents elicited in ND7/23 cells expressing $hNa_V1.9$-GFP by a 50-ms depolarization to −50 mV from a holding potential of −120 mV. One micro molar TTX were applied in all experiments.

REFERENCES

Adams, G. K., Lichtenstein, L. (1979). *In vitro* studies of antigen-induced bronchospasm: effect of antihistamine and SRS-A antagonist on response of sensitized guinea pig and human airways to antigen. *J. Immunol.* 122, 555–562.

Amaya, F., Wang, H., Costigan, M., Allchorne, A. J., Hatcher, J. P., Egerton, J., et al. (2006). The voltage-gated sodium channel Na(v)1.9 is an effector of peripheral inflammatory pain hypersensitivity. *J. Neurosci. Offic. J. Soc. Neurosci.* 26, 12852–12860. doi: 10.1523/JNEUROSCI.4015-06.2006

Armstrong, C. M. (2006). Na channel inactivation from open and closed states. *Proc. Natl. Acad. Sci. U.S.A.* 103, 17991–17996. doi: 10.1073/pnas.0607603103

Bähring, R., and Covarrubias, M. (2011). Mechanisms of closed-state inactivation in voltage-gated ion channels. *J. Physiol.* 589, 461–479. doi: 10.1113/jphysiol.2010.191965

Baker, M. D., Chandra, S. Y., Ding, Y., Waxman, S. G., and Wood, J. N. (2003). GTP-induced tetrodotoxin-resistant Na+ current regulates excitability in mouse and rat small diameter sensory neurones. *J. Physiol.* 548, 373–382. doi: 10.1113/jphysiol.2003.039131

Bant, J. S., and Raman, I. M. (2010). Control of transient, resurgent, and persistent current by open-channel block by Na channel beta4 in cultured cerebellar granule neurons. *Proc. Natl. Acad. Sci. U.S.A.* 107, 12357–12362. doi: 10.1073/pnas.1005633107

Benbarek, H., Mouithys-Mickalad, A., Deby-Dupont, G., Deby, C., Grülke, S., Nemmar, A., et al. (1999). High concentrations of histamine stimulate equine polymorphonuclear neutrophils to produce reactive oxygen species. *Inflamm. Res.* 48, 594–601. doi: 10.1007/s000110050509

Catterall, W. A. (2000). From ionic currents to molecular mechanisms: the structure and function of voltage-gated sodium channels. *Neuron* 26, 13–25. doi: 10.1016/S0896-6273(00)81133-2

Catterall, W. A. (2012). Voltage-gated sodium channels at 60: structure, function and pathophysiology. *J. Physiol.* 590, 2577–2589. doi: 10.1113/jphysiol.2011.224204

Catterall, W. A. (2014). Structure and function of voltage-gated sodium channels at atomic resolution. *Exp. Physiol.* 99, 35–51. doi: 10.1113/expphysiol.2013.071969

Catterall, W. A. (2015). Finding Channels. *J. Biol. Chem.* 290, 28357–28373. doi: 10.1074/jbc.X115.683383

Cummins, T. R., Dib-Hajj, S. D., Black, J. A., Akopian, A. N., Wood, J. N., and Waxman, S. G. (1999). A novel persistent tetrodotoxin-resistant sodium current in SNS-null and wild-type small primary sensory neurons. *J. Neurosci.* 19:RC43.

Cummins, T. R., Howe, J. R., and Waxman, S. G. (1998). Slow closed-state inactivation: a novel mechanism underlying ramp currents in cells expressing the hNE/PN1 sodium channel. *J. Neurosci.* 18, 9607–9619.

Dib-Hajj, S., Black, J. A., Cummins, T. R., and Waxman, S. G. (2002). NaN/Nav1.9: a sodium channel with unique properties. *Trends Neurosci.* 25, 253–259. doi: 10.1016/S0166-2236(02)02150-1

Dib-Hajj, S. D., Black, J. A., and Waxman, S. G. (2015). NaV1. 9: a sodium channel linked to human pain. *Nat. Rev. Neurosci.* 16, 511–519. doi: 10.1038/nrn3977

Dray, A. (1995). Inflammatory mediators of pain. *Br. J. Anaesth.* 75, 125–131. doi: 10.1093/bja/75.2.125

Ekberg, J., Jayamanne, A., Vaughan, C. W., Aslan, S., Thomas, L., Mould, J., et al. (2006). muO-conotoxin MrVIB selectively blocks Nav1.8 sensory neuron specific sodium channels and chronic pain behavior without motor deficits. *Proc. Natl. Acad. Sci. U.S.A.* 103, 17030–17035. doi: 10.1073/pnas.0601819103

Fozzard, H. A., Lee, P. J., and Lipkind, G. M. (2005). Mechanism of local anesthetic drug action on voltage-gated sodium channels. *Curr. Pharm. Des.* 11, 2671–2686. doi: 10.2174/1381612054546833

Goral, R. O., Leipold, E., Nematian-Ardestani, E., and Heinemann, S. H. (2015). Heterologous expression of NaV1.9 chimeras in various cell systems. *Pflug. Archiv.* 467, 2423–2435. doi: 10.1007/s00424-015-1709-1

Gorelova, N., and Reiner, P. B. (1996). Histamine depolarizes cholinergic septal neurons. *J. Neurophysiol.* 75, 707–714.

Haas, H., and Panula, P. (2003). The role of histamine and the tuberomamillary nucleus in the nervous system. *Nat. Rev. Neurosci.* 4, 121–130. doi: 10.1038/nrn1034

Han, C., Yang, Y., de Greef, B. T., Hoeijmakers, J. G., Gerrits, M. M., Verhamme, C., et al. (2015). The domain II S4-S5 linker in Nav1.9: a missense mutation enhances activation, impairs fast inactivation, and produces human painful neuropathy. *Neuromol. Med.* 17, 158–169. doi: 10.1007/s12017-015-8347-9

Han, C., Yang, Y., Te Morsche, R. H., Drenth, J. P., Politei, J. M., Waxman, S. G., et al. (2017). Familial gain-of-function $Na_V1.9$ mutation in a painful channelopathy. *J. Neurol. Neurosurg. Psychiatry* 88, 233–240. doi: 10.1136/jnnp-2016-313804

Herzog, R. I., Cummins, T. R., and Waxman, S. G. (2001). Persistent TTX-resistant Na+ current affects resting potential and response to depolarization in simulated spinal sensory neurons. *J. Neurophysiol.* 86, 1351–1364.

Hockley, J. R., Boundouki, G., Cibert-Goton, V., McGuire, C., Yip, P. K., Chan, C., et al. (2014). Multiple roles for NaV1.9 in the activation of visceral afferents by noxious inflammatory, mechanical, and human disease-derived stimuli. *Pain* 155, 1962–1975. doi: 10.1016/j.pain.2014.06.015

Hoerbelt, P., Ramerstorfer, J., Ernst, M., Sieghart, W., Thomson, J. L., Hough, L. B., et al. (2016). Mutagenesis and computational docking studies support the existence of a histamine binding site at the extracellular beta3+beta3-interface of homooligomeric beta3 GABAA receptors. *Neuropharmacology* 108, 252–263. doi: 10.1016/j.neuropharm.2016.04.042

Huang, J., Han, C., Estacion, M., Vasylyev, D., Hoeijmakers, J. G., Gerrits, M. M., et al. (2014). Gain-of-function mutations in sodium channel NaV1. 9 in painful neuropathy. *Brain* 137, 1627–1642. doi: 10.1093/brain/awu079

Huang, J., Vanoye, C. G., Cutts, A., Goldberg, Y. P., Dib-Hajj, S. D., Cohen, C. J., et al. (2017). Sodium channel NaV1.9 mutations associated with insensitivity to pain dampen neuronal excitability. *J. Clin. Invest.* 127, 2805–2814. doi: 10.1172/JCI92373

Imbrici, P., Liantonio, A., Camerino, G. M., De Bellis, M., Camerino, C., Mele, A., et al. (2016). Therapeutic approaches to genetic ion channelopathies and perspectives in drug discovery. *Front. Pharmacol.* 7:121. doi: 10.3389/fphar.2016.00121

Kajihara, Y., Murakami, M., Imagawa, T., Otsuguro, K., Ito, S., and Ohta, T. (2010). Histamine potentiates acid-induced responses mediating transient receptor potential V1 in mouse primary sensory neurons. *Neuroscience* 166, 292–304. doi: 10.1016/j.neuroscience.2009.12.001

Leipold, E., Hanson-Kahn, A., Frick, M., Gong, P., Bernstein, J. A., Voigt, M., et al. (2015). Cold-aggravated pain in humans caused by a hyperactive NaV1.9 channel mutant. *Nat. Commun.* 6:10049. doi: 10.1038/ncomms10049

Leipold, E., Liebmann, L., Korenke, G. C., Heinrich, T., Gießelmann, S., Baets, J., et al. (2013). A de novo gain-of-function mutation in SCN11A causes loss of pain perception. *Nat. Genet.* 45, 1399–1404. doi: 10.1038/ng.2767

Lin, Z., Santos, S., Padilla, K., Printzenhoff, D., and Castle, N. A. (2016). Biophysical and pharmacological characterization of nav1.9 voltage dependent sodium channels stably expressed in HEK-293 Cells. *PLoS ONE* 11:e0161450. doi: 10.1371/journal.pone.0161450

Lolignier, S., Amsalem, M., Maingret, F., Padilla, F., Gabriac, M., Chapuy, E., et al. (2011). Nav1.9 channel contributes to mechanical and heat pain hypersensitivity induced by subacute and chronic inflammation. *PLoS ONE* 6:e23083. doi: 10.1371/journal.pone.0023083

Lolignier, S., Bonnet, C., Gaudioso, C., Noël, J., Ruel, J., Amsalem, M., et al. (2015). The Nav1. 9 channel is a key determinant of cold pain sensation and cold allodynia. *Cell Rep.* 11, 1067–1078. doi: 10.1016/j.celrep.2015.04.027

Maingret, F., Coste, B., Padilla, F., Clerc, N., Crest, M., Korogod, S. M., et al. (2008). Inflammatory mediators increase Nav1.9 current and excitability in nociceptors through a coincident detection mechanism. *J. Gen. Physiol.* 131, 211–225. doi: 10.1085/jgp.200709935

Mobarakeh, J. I., Sakurada, S., Katsuyama, S., Kutsuwa, M., Kuramasu, A., Lin, Z. Y., et al. (2000). Role of histamine H(1) receptor in pain perception: a study of the receptor gene knockout mice. *Eur. J. Pharmacol.* 391, 81–89. doi: 10.1016/S0014-2999(00)00060-1

Nagaeva, E. I., Tikhonova, T. B., Magazanik, L. G., and Tikhonov, D. B. (2016). Histamine selectively potentiates acid-sensing ion channel 1a. *Neurosci. Lett.* 632, 136–140. doi: 10.1016/j.neulet.2016.08.047

Okuda, H., Noguchi, A., Kobayashi, H., Kondo, D., Harada, K. H., Youssefian, S., et al. (2016). Infantile pain episodes associated with novel nav1.9 mutations in familial episodic pain syndrome in japanese families. *PLoS ONE* 11:e0154827. doi: 10.1371/journal.pone.0154827

Ostman, J. A., Nassar, M. A., Wood, J. N., and Baker, M. D. (2008). GTP up-regulated persistent Na+ current and enhanced nociceptor excitability require NaV1.9. *J. Physiol.* 586, 1077–1087. doi: 10.1113/jphysiol.2007.147942

Padilla, F., Couble, M. L., Coste, B., Maingret, F., Clerc, N., Crest, M., et al. (2007). Expression and localization of the Nav1.9 sodium channel in enteric neurons and in trigeminal sensory endings: implication for intestinal reflex function and orofacial pain. *Mol. Cell. Neurosci.* 35, 138–152. doi: 10.1016/j.mcn.2007.02.008

Penzotti, J. L., Fozzard, H. A., Lipkind, G. M., and Dudley, S. C. Jr. (1998). Differences in saxitoxin and tetrodotoxin binding revealed by mutagenesis of the Na^+ channel outer vestibule. *Biophys. J.* 75, 2647–2657. doi: 10.1016/S0006-3495(98)77710-0

Phatarakijnirund, V., Mumm, S., McAlister, W. H., Novack, D. V., Wenkert, D., Clements, K. L., et al. (2016). Congenital insensitivity to pain: fracturing without apparent skeletal pathobiology caused by an autosomal dominant, second mutation in SCN11A encoding voltage-gated sodium channel 1.9. *Bone* 84, 289–298. doi: 10.1016/j.bone.2015.11.022

Priest, B. T., Murphy, B. A., Lindia, J. A., Diaz, C., Abbadie, C., Ritter, A. M., et al. (2005). Contribution of the tetrodotoxin-resistant voltage-gated sodium channel NaV1.9 to sensory transmission and nociceptive behavior. *Proc. Natl. Acad. Sci. U.S.A.* 102, 9382–9387. doi: 10.1073/pnas.0501549102

Rogers, M., Zidar, N., Kikelj, D., and Kirby, R. W. (2016). Characterization of endogenous sodium channels in the ND7-23 neuroblastoma cell line: implications for use as a heterologous ion channel expression system suitable for automated patch clamp screening. *Assay Drug Dev. Technol.* 14, 109–130. doi: 10.1089/adt.2016.704

Rush, A. M., and Waxman, S. G. (2004). PGE2 increases the tetrodotoxin-resistant Nav1.9 sodium current in mouse DRG neurons via G-proteins. *Brain Res.* 1023, 264–271. doi: 10.1016/j.brainres.2004.07.042

Saras, A., Gisselmann, G., Vogt-Eisele, A. K., Erlkamp, K. S., Kletke, O., Pusch, H., et al. (2008). Histamine action on vertebrate GABAA receptors: direct channel gating and potentiation of GABA responses. *J. Biol. Chem.* 283, 10470–10475. doi: 10.1074/jbc.M709993200

Thiel, U., Platt, S. J., Wolf, S., Hatt, H., and Gisselmann, G. (2015). Identification of amino acids involved in histamine potentiation of GABA A receptors. *Front. Pharmacol.* 6:106. doi: 10.3389/fphar.2015.00106

Vanoye, C. G., Kunic, J. D., Ehring, G. R., and George, A. L. (2013). Mechanism of sodium channel NaV1. 9 potentiation by G-protein signaling. *J. Gen. Physiol.* 141, 193–202. doi: 10.1085/jgp.201210919

Woods, C. G., Babiker, M. O., Horrocks, I., Tolmie, J., and Kurth, I. (2015). The phenotype of congenital insensitivity to pain due to the NaV1.9 variant p.L811P. *Eur. J. Hum. Genet.* 23, 561–563. doi: 10.1038/ejhg.2014.166

Woolf, C. J., and Ma, Q. (2007). Nociceptors–noxious stimulus detectors. *Neuron* 55, 353–364. doi: 10.1016/j.neuron.2007.07.016

Yu, J., Fang, Q., Lou, G. D., Shou, W. T., Yue, J. X., Tang, Y. Y., et al. (2013). Histamine modulation of acute nociception involves regulation of Nav 1.8 in primary afferent neurons in mice. *CNS Neurosci. Ther.* 19, 649–658. doi: 10.1111/cns.12134

Yue, J. X., Wang, R. R., Yu, J., Tang, Y. Y., Hou, W. W., Lou, G. D., et al. (2014). Histamine upregulates Nav1.8 expression in primary afferent neurons via H2 receptors: involvement in neuropathic pain. *CNS Neurosci. Ther.* 20, 883–892. doi: 10.1111/cns.12305

Zhang, X. Y., Wen, J., Yang, W., Wang, C., Gao, L., Zheng, L. H., et al. (2013). Gain-of-function mutations in SCN11A cause familial episodic pain. *Am. J. Hum. Genet.* 93, 957–966. doi: 10.1016/j.ajhg.2013.09.016

Zhou, X., Dong, X. W., Crona, J., Maguire, M., and Priestley, T. (2003). Vinpocetine is a potent blocker of rat NaV1.8 tetrodotoxin-resistant sodium channels. *J. Pharmacol. Exp. Ther.* 306, 498–504. doi: 10.1124/jpet.103.051086

Conflict of Interest Statement: The authors declare that the research was conducted in the absence of any commercial or financial relationships that could be construed as a potential conflict of interest.

The reviewer TM and handling Editor declared their shared affiliation.